Optimization of Microbubble Concentration and Acoustic Pressure for Left Ventricular High-Frame-Rate EchoPIV in Patients

Jason Voorneveld, Lana B. H. Keijzer, Mihai Strachinaru, Daniel J. Bowen, Ferit Onur Mutluer, Antonius F. W. van der Steen, *Fellow, IEEE*, Folkert J. Ten Cate, Nico de Jong, *Member, IEEE*, Hendrik J. Vos, *Member, IEEE*, Annemien E. van den Bosch, and Johan G. Bosch, *Member, IEEE*

Abstract—**High-frame-rate (HFR) echo-particle image velocimetry (echoPIV) is a promising tool for measuring intracardiac blood flow dynamics. In this study, we investigate the optimal ultrasound contrast agent (UCA: SonoVue) infusion rate and acoustic output to use for HFR echoPIV (PRF = 4900 Hz) in the left ventricle (LV) of patients. Three infusion rates (0.3, 0.6, and 1.2 ml/min) and five acoustic output amplitudes (by varying transmit voltage: 5, 10, 15, 20, and 30 V—corresponding to mechanical indices of 0.01, 0.02, 0.03, 0.04, and 0.06 at 60-mm depth) were tested in 20 patients admitted for symptoms of heart failure. We assess the accuracy of HFR echoPIV against pulsed-wave Doppler acquisitions obtained for mitral inflow and aortic outflow. In terms of image quality, the 1.2-ml/min infusion rate provided the highest contrast-to-background ratio (CBR) (3-dB improvement over 0.3 ml/min). The highest acoustic output tested resulted in the lowest CBR. Increased acoustic output also resulted in increased microbubble disruption. For the echoPIV results, the 1.2-ml/min infusion rate provided the best vector quality and accuracy; mid-**

range acoustic outputs (corresponding to 15–20-V transmit voltages) provided the best agreement with the pulsed-wave Doppler. Overall, the highest infusion rate (1.2 ml/min) and mid-range acoustic output amplitudes provided the best image quality and echoPIV results.

I. INTRODUCTION

BLOOD flow in the left ventricle (LV) is an important diagnostic marker for heart failure. The most widely used modality for assessing LV blood flow is echocardiography, where ultrasound Doppler is used to measure the blood velocity. However, the main limitation of ultrasound Doppler-based methods is that only the velocity component in the direction of the wave propagation can be measured, the cross-beam components can only be recovered if the velocity angle is known, and the beam-to-flow angle is moderate ($<60°–70°$ [1]). For flow in the LV, these conditions are only satisfied when measuring flow through the mitral valve (MV) and aortic outflow tract, whereas the angle of flow within the LV chamber changes over space and time.

Some echocardiographic techniques are able to estimate both the magnitude and direction of the blood velocity vectors, which we collectively name *vector flow imaging* (VFI) techniques—prominent examples include: *Transverse Oscillations*, which use receive apodization to create a laterally oscillating field that can be used for lateral displacement estimation [2], [3]; *Vector Flow Mapping*, which calculates the lateral velocity component by postprocessing color Doppler acquisitions [4]; *Blood Speckle Tracking,* which estimates the displacement of the speckle patterns arising from red blood cell backscatter using block-matching [5]–[7]; and *Echo-Particle Image Velocimetry* (echoPIV—also known as ultrasound image velocimetry), which also tracks speckle patterns but those arising from ultrasound contrast agent (UCA) microbubbles that have been injected intravenously into the bloodstream [8]–[11].

Clinically approved UCAs are typically $1–10$-μm diameter microbubbles consisting of a gas encapsulated in a

lipid shell-featuring a backscatter power orders of magnitude stronger than red blood cells, allowing for improved blood opacification and SNR over native blood imaging. This SNR improvement gives echoPIV an advantage over the other VFI techniques in cardiac applications, where limited transducer aperture, large imaging depths, and high velocity flows complicate measurement.

Typically, specialized pulsing schemes are used for contrast-enhanced ultrasound (CEUS), such as pulse inversion (PI [12], [13]), which suppress tissue signal while retaining the microbubble signal, greatly reducing clutter, which would otherwise interfere with visualizing the blood pool.

Recent developments in echoPIV have used high-frame-rate (HFR) CEUS, utilizing plane-wave [14], [15] or diverging-wave acquisition schemes [16]–[21] instead of the focused beam-scanning schemes used on clinical scanners. This has overcome one of the key limitations of conventional echoPIV research: the severe underestimation of velocities higher than $\sim$40 cm/s [22]–[24].

We have shown previously that HFR echoPIV can indeed measure the high velocity flows present in the LV *in vitro* [16] and in a patient [21]. However, the optimal UCA settings for LV VFI, such as microbubble concentration and applied acoustic pressure, have yet to be determined. It is known from conventional CEUS imaging that too low UCA concentrations result in insufficient opacification of the blood pool, while too high concentrations can result in imaging artifacts and significant attenuation, limiting visualization of deeper regions [25], [26]. In terms of applied acoustic pressure, previous studies have shown that diverging/plane wave acquisitions should use very low acoustic pressures to prevent microbubble disruption [20], [27]–[29], but it is also expected that if acoustic pressure is too low then SNR will be insufficient for echoPIV processing.

In this study, we investigate the effect of UCA infusion rate (concentration) and acoustic pressure (by varying transmit voltage) on image quality and VFI quality and peak velocity accuracy when using HFR CEUS in 20 patients.

II. METHODS

A. Patient Selection and Experimental Design

After approval by the institutional review board of the Erasmus University Medical Center (NL63755.078.18), 20 patients were included who presented to the hospital with symptoms of heart failure. A wide variety of pathologies were included to test feasibility under clinically relevant imaging circumstances (details in Table I).

Patients were first imaged with a clinical ultrasound machine (EPIQ 7, Philips Healthcare, Best, The Netherlands) and probe (X5-1, Philips Healthcare) to obtain B-mode and color Doppler sequences of the LV in an apical three-chamber view (see Fig. 1). In addition, pulsed-wave (PW) Doppler sequences were acquired in the regions of the MV tips and the left-ventricular outflow tract (LVOT), aligning the probe beam with the principal flow direction as best as possible.

Next, a diluted solution of UCA (SonoVue, Bracco Imaging SpA, Milan, Italy; 5-ml SonoVue diluted with 15-ml isotonic

TABLE I
PATHOLOGICAL CLASSIFICATION OF PATIENTS INCLUDED IN STUDY WITH SELECTED DETAILS, INCLUDING: NUMBER INCLUDED (N), SEX (M/F), BODY MASS INDEX (BMI), EJECTION FRACTION (EF), AND AGE. METRICS ARE SHOWN AS MEDIAN (RANGE)

Pathology	N	M/F	BMI	EF [%]	Age [Years]
Dilated Cardiomyopathy					
- Ischemic	5	4/1	24 (20-28)	25 (18-50)	71 (63-78)
- Non-ischemic	5	3/2	23 (20-27)	38 (20-45)	59 (19-69)
- Takotsubo	1	0/1	16	50	72
Hypertrophic Cardiomyopathy	3	1/2	29 (24-34)	45 (40-60)	51 (47-63)
Restrictive Cardiomyopathy	2	0/2	25 (20-30)	53 (45-60)	67 (64-70)
Other					
- Arrhythmia	2	2/0	26 (23-29)	43 (40-45)	40 (18-62)
- Constrictive pericarditis	1	1/0	22	70	65
Normal function	1	1/0	29	60	60

Pathological classification of patients included in study with selected details, including: number included (N), sex (M/F), body mass index (BMI), ejection fraction (EF) and Age. Metrics are shown as median (range).
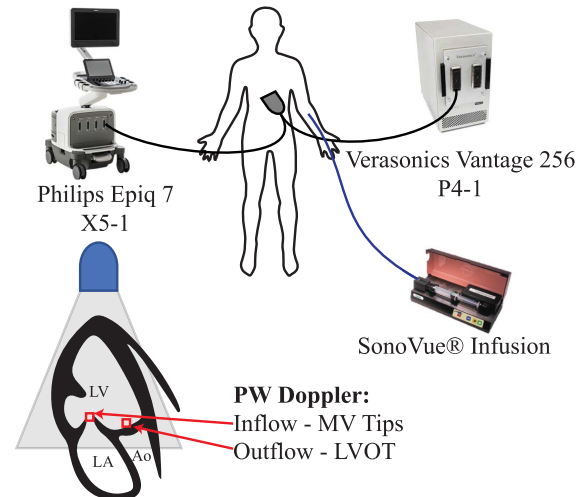
Fig. 1. Diagrammatic overview of the experiment: first, the patients are imaged with the clinical system (Philips), obtaining inflow and outflow PW Doppler spectra, and then, the HFR CEUS acquisitions are acquired (after UCA infusion) using the research system (Verasonics).

saline) was intravenously infused using a continuous infusion pump (VueJect BR-INF 100, Bracco Imaging SpA) using the recommended infusion kit (20-ml syringe, Original-Perfusor, B. Braun, Hessen, Germany; 20-G needle, Pikdare, CO, Italy; and connection line: $\varnothing_i = 0.55$ mm, L = 910 mm, Sidam, MO, Italy). Three different infusion rates were tested (in order): 1.2, 0.6, and 0.3 ml/min (of the diluted UCA solution, not adjusted for weight). The arrival and stabilization of the contrast concentration were observed using the contrast mode of the clinical ultrasound machine before switching to the research system for HFR CEUS acquisitions. The HFR CEUS imaging sequences (see Section II-B) were acquired in an apical three-chamber view using a research ultrasound system (Vantage 256, Verasonics, Kirkland, WA, USA) with a phased-array probe (P4-1, ATL). A separate line-scanning mode with real-time beamforming was used to align anatomical

TABLE II
CEUS PARAMETERS TESTED

CEUS Parameters Tested				
Contrast infusion rates (in order)				
1.2 ml/min		0.6 ml/min		0.3 ml/min
Transmit Voltages (in order)				
5 V	10 V	15 V	20 V	30 V
Imaging Parameters				
Parameter	Value			
PRF	4900 Hz			
Transmit angles	2 (-7°, 7°)			
Virtual focus radius	-47 mm			
Probe	P4-1			
Probe aperture	28.3 mm			
CEUS mode	Pulse Inversion			
Pulse type	Gaussian tapered sinusoid			
Pulse centre frequency	1.5 MHz			
Pulse cycles	2			
Pixel size	0.31° x 308 µm			
EchoPIV Parameters				
Pre-processing				
Fast-time (harmonic) filter:	4th order Butterworth (2.6-3.8 MHz)			
Slow-time (wall) filter:	4th order Butterworth high-pass (100 Hz)			
Boundary mask	Manually drawn (static)			
PIV processing				
Number of Iterations	4			
Window deformation	Bilinear			
Window Size:				
- Iteration 1	10° x 10 mm (32 x 32 px)			
- Iteration 2	10° x 10 mm (32 x 32 px)			
- Iteration 3	5° x 5 mm (16 x 16 px)			
- Iteration 4	5° x 5 mm (16 x 16 px)			
Overlap	75%			
- Final grid size	1.25° x 1.25 mm			
Correlation averaging	(2 x angles) x (10 x frames) = 20 (~8ms)			
Sub-pixel fitting	2x3 point parabolic fit			
Post-processing				
Spatial smoothing	2D Gaussian (σ≈0.6 mm, extent≈4mm)			
Temporal smoothing	3 ensemble moving average (~24ms)			

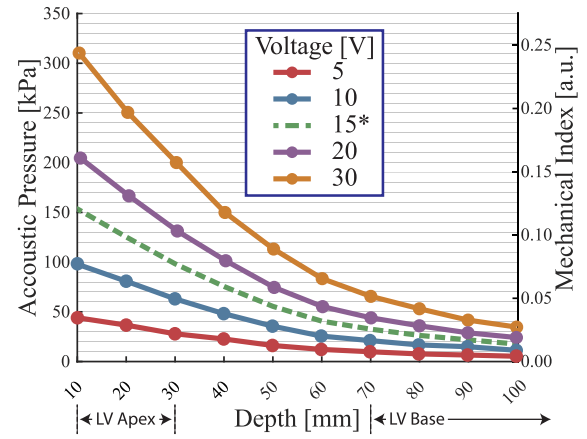Contrast enhanced ultrasound (CEUS) parameters tested and imaging/echoPIV parameters used in this study.

Fig. 2. Hydrophone measured pressure (left axis) and mechanical index (MI, right axis) as a function of transmit voltage and depth. *15-V data interpolated from 10- and 20-V measured data (circular markers). LV Apex and LV Base indicate the typical depths of the LV apex and base when imaging in the apical three-chamber view. The LV base can extend up to 15 cm with larger ventricles.

The depth of imaging was limited to 12 cm (sufficient for normal LVs, although larger dilated LVs may require ~15 cm), and maximal obtainable pulse repetition frequency (PRF) was 4900 Hz, providing an effective frame rate of 1225 frames/s. A total of 2.5 s was captured per acquisition, allowing for at least two cardiac cycles to be recorded.
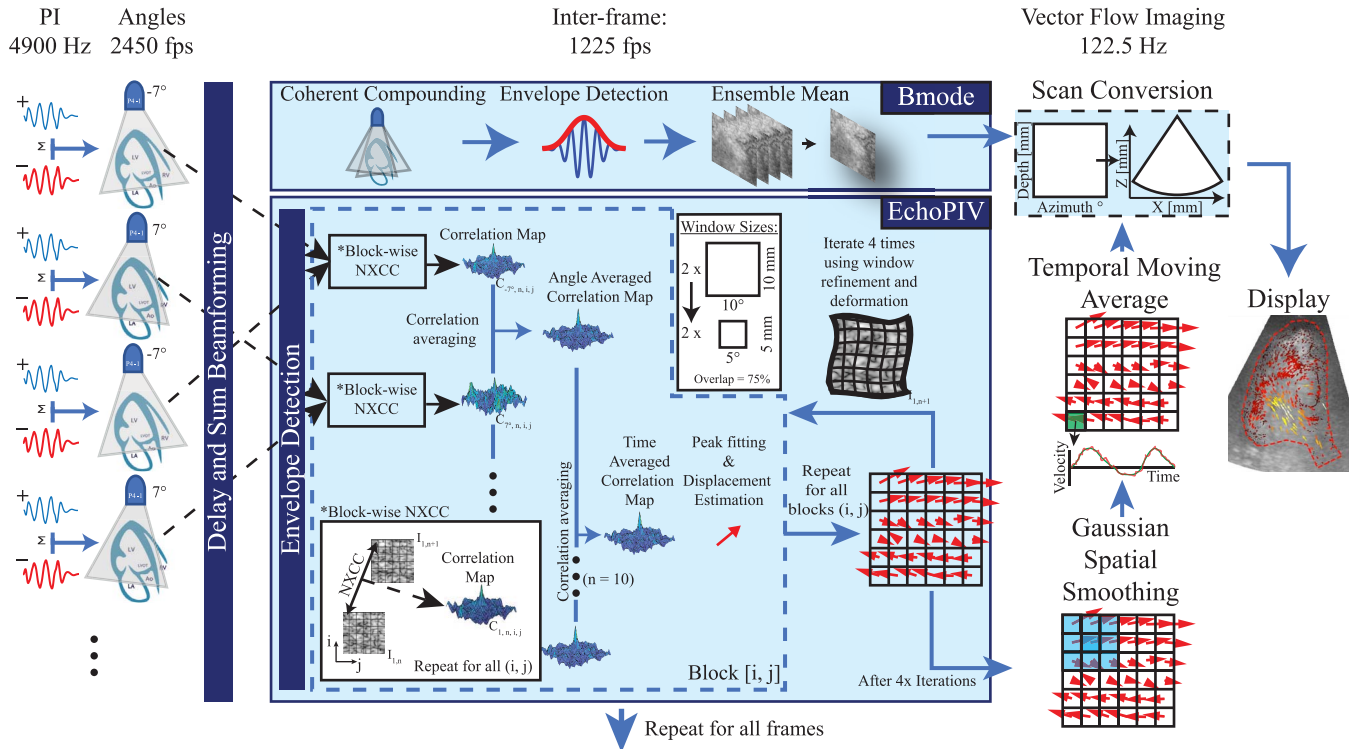
In the off-line, saved RF data were passed through a fast-time fourth-order Butterworth bandpass filter (2.6–3.8 MHz) to remove the fundamental frequency component remaining after imperfect PI cancellation. The filtered data were then beamformed onto a polar coordinate system, using the Verasonics software beamformer. A fourth-order Butterworth high-pass (100-Hz~3-cm/s axially) slow-time filter was then used to remove low-frequency tissue clutter.

The polar beamformed IQ data were used for echoPIV processing before performing coherent compounding (see Section II-C). For the B-mode images used in the final vector flow visualizations, coherent compounding was performed, as well as ten-frame ensemble-averaging after envelope detection—to match the frame rate of the resulting echoPIV results.

C. EchoPIV Processing

A PIV algorithm employing iterative window refinement and deformation, developed in MATLAB (R2019a, Math-Works, Natick, MA, USA), was used for velocity estimation on the beamformed polar domain data after envelope detection (further developed from [16], [18], and [20]).

This PIV algorithm divided the image area into equally sized blocks with an overlap; then, normalized cross correlation (NXCC) was computed (in the frequency domain) on blocks between subsequent frames, and the peak of each correlation function was used (after subpixel fitting) to obtain the displacement between the two frames per block. The iterative part of the algorithm attempts to reduce bias in the displacement estimation by performing the blockwise NXCC step multiple times, using the displacements calculated in

landmarks on the research system with those acquired with the clinical system. Five different transmit voltages (in order: 5, 10, 15, 20, and 30 V) were tested per UCA infusion rate. After obtaining HFR CEUS acquisitions for all transmit voltage for a given infusion rate, the infusion rate was reduced, and the clinical system was used to visually confirm that the new concentration level had been reached before obtaining the next set of HFR CEUS acquisitions. Table II lists the infusion rates and transmit voltages investigated.

The whole experimental protocol took approximately 30 min and an extra 15 min if a cannula needed to be inserted into the patient.

The acoustic pressures (measured using a hydrophone in the water and adjusting for 0.3-dB/cm·MHz attenuation) of each transmit voltage are plotted in Fig. 2.

B. HFR CEUS Imaging Sequence

The HFR CEUS imaging consisted of four repeated diverging-wave acquisitions: two alternating polarity transmits (PI, F_c = 1.5 MHz) at two different angles (+7°, −7°).

Fig. 3. Block diagram of echoPIV processing pipeline, including B-mode image processing for visualization of vector flow results. NXCC = normalized cross correlation. See Section II-C for details.

the previous iteration to deform the target frame by the displacement field (thereby iteratively reducing the displacement between frames toward zero) [30]. Between iterations, the window size is also reduced to increase the resolution and further reduce the bias of the calculated displacement field (Table II—PIV processing).

Instead of performing coherent compounding with the angular acquisitions, correlation compounding was used, where the blockwise normalized cross correlation was performed between like-angles and the resulting correlation maps averaged across the different angles [16]. In addition, correlation averaging across an ensemble of ten frames was used to further reduce noise.

Furthermore, a 2-D Gaussian spatial smoothing filter and ensemble temporal moving average filter were applied to the computed velocity fields (Table II—postprocessing). Finally, the velocity data were scan converted for visualization using the vector projectile imaging technique [31] (see Fig. 3 for a diagrammatic overview of the process).

D. Methods of Analysis

Four different metrics were assessed to determine which combinations of CEUS parameters were most favorable for echoPIV processing: 1) contrast-to-background ratio (CBR) that estimates the signal power of microbubbles in relation to the unwanted background signal (be it tissue backscatter or noise) 2) microbubble disruption where a large degree of disruption would be counterproductive for tracking the microbubbles over time; 3) qualitative assessment of the vector tracking results; and 4) accuracy of the echoPIV estimated vectors, using the peak early filling velocities from the PW

Doppler spectra as a reference value. Each method is described in more detail in the following.

1) Contrast-to-Background Ratio: CBR was estimated as the mean signal power inside the LV cavity relative to the mean signal power of a 7.5-mm surrounding section (approximating the LV myocardium), over the whole acquisition duration. This assumes that the UCA concentration is negligible in the myocardium. CBR was calculated as follows:

$$\text{CBR} = 20 \log_{10} \frac{\text{mean}\left(|\text{IQ}_{\text{LV Cavity}}|\right)}{\text{mean}\left(|\text{IQ}_{\text{LV myocardium}}|\right)}. \tag{1}$$

2) Microbubble Disruption: Microbubble disruption was assessed by quantifying the intracavity signal power decrease over the first 20 frames (16 ms), using only the 1.2-ml/min contrast infusion rate. We limited the analysis to the first 20 frames (80 acquisitions, including PI and two angles) to observe the change in microbubble response at the onset of HFR imaging.

3) Qualitative Assessment Criteria: EchoPIV tracking quality was assessed by visually judging and scoring the vector flow visualizations according to a predetermined set of criteria (rubric—see Table III). Intraobserver and interobserver reliabilities for the scoring were assessed by repeating the assessment on a subset of the patients ($n = 4$, two nonmedically trained but experienced observers: J. V. & J. G. B.) and calculating Cohen's kappa statistic.

4) Comparison to PW Doppler: The ability of echoPIV to accurately estimate high velocities was assessed by regression analysis of the peak filling and ejection velocities measured using echoPIV with those measured using conventional PW Doppler. For the PW Doppler acquisitions, the filling was

TABLE III
QUALITATIVE ASSESSMENT RUBRIC

Criteria	Score		
	0	1	2
Clutter	Major interference with flow (> 1 position)	Minor interference with flow (1 position)	No clutter or no interference
Inflow	Not visible	Visible but noisy/underestimated (<70% PW Doppler)	Visible, smooth and in correct velocity range
Outflow	Not visible	Visible but noisy/underestimated (<70% PW Doppler)	Visible, smooth and in correct velocity range
Apical Flow	Not visible	Visible but noisy / not tracking bubbles	Visible, smooth and tracking bubble motion
Middle Flow	Not visible	Visible but noisy / not tracking bubbles	Visible, smooth and tracking bubble motion

Qualitative criteria for visual assessment of echoPIV tracking quality. There are 5 criteria each with a maximal score of 2 and a maximum total score of 10.
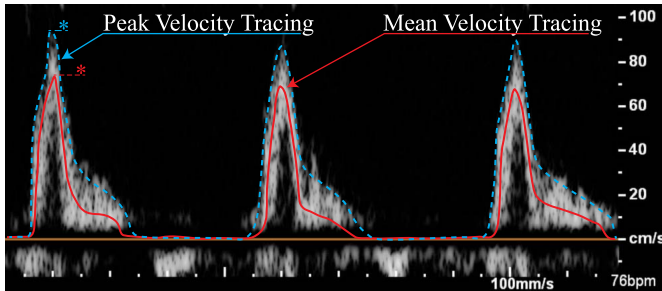

Fig. 4. Example of the peak (blue dashed curve) and mean (solid red curve) velocity tracings of the PW Doppler spectra. The maxima (*) of each over the acquired heartbeats were used for the quantitative comparison with the peak echoPIV results.

measured between the MV tips, and ejection was measured in the LVOT (see Fig. 1).

Two tracings were approximated for each PW Doppler spectrum: 1) the peak envelope of the spectrum and 2) the tracing of maximum power (see Fig. 4). The sampling area for echoPIV was adjusted to match the PW Doppler range-gate and position as closely as possible.

A single ejection/filling period was manually chosen for each echoPIV acquisition to reduce the effect of noise. If filling or ejection could not be seen in an acquisition (because of acoustic shadowing, planar misalignment, or insufficient imaging depth), then the acquisition was excluded from the linear regression analysis.

E. Statistics

Data normality (of residuals) and equivariance were assessed using the Shapiro–Wilk test and Bartlett's test, respectively.

Differences in CBR (see Section III-A1) were assessed using a Welch one-way ANOVA (data residuals normally distributed but not homoscedastic) followed by *post hoc* Games–Howell tests.
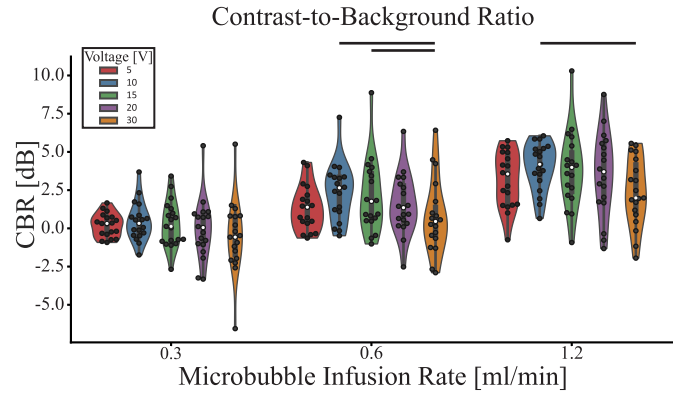

Fig. 5. CBR increases with the UCA infusion rate, but a transmit voltage of 10 V provides the highest CBR on average. Violin plots indicate kernel density estimates of the data points (black dots). White circles indicate the median. Black horizontal bars indicate statistically significant differences. See Section III-A1 for details.

TABLE IV
CONTRAST TO BACKGROUND RATIO (CBR) [dB]

	0.3 ml/min	0.6 ml/min	1.2 ml/min	All
5V	0.2 [-0.2, 0.6]	1.3 [0.6, 2.0]	3.2 [2.3, 4.0]	1.6 [1.1, 2.1]
10V	0.4 [-0.2, 1.0]	2.4 [1.5, 3.3]	4.0 [3.3, 4.8]	2.3 [1.7, 2.9]
15V	0.3 [-0.4, 1.0]	2.1 [0.9, 3.2]	3.8 [2.7, 5.0]	2.1 [1.4, 2.8]
20V	-0.1 [-1.0, 0.9]	1.5 [0.6, 2.5]	3.5 [2.3, 4.8]	1.7 [1.0, 2.4]
30V	-0.5 [-1.7, 0.6]	0.7 [-0.4, 1.9]	2.4 [1.3, 3.4]	0.9 [0.2, 1.5]
All	-0.1 [-0.3, 0.4]	1.6 [1.2, 2.0]	3.4 [2.9, 3.8]	1.7 [1.4, 2.0]

Mean [95% CI] CBRs across groups and their aggregates.

Microbubble disruption (see Section III-A2) was assessed using a two-way repeated measures ANOVA over time and transmit voltage.

Differences in qualitative scoring (see Section III-B1) were assessed using a Kruskal–Wallis test between concentration groups and voltages independently (data with nonnormally distributed residuals but homoscedastic), followed by *post hoc* Dunn's tests.

The null hypothesis was rejected for p-values < 0.05. The mean and the bounds of the 95% confidence interval (CI) are reported in the text as mean [95% confidence limits].

III. RESULTS

Out of the 20 patients included in the study, one patient chose to end participation before UCA infusion. The 12-cm-depth limit was sufficient for all but three patients, whose larger LVs required greater imaging depths to include the MV and LVOT; however, the flow could still be observed in the LV chamber for those patients.

A. Image Quality

1) Contrast-to-Background Ratio: The CBR results are tabulated in Table IV and displayed in Fig. 5. Higher microbubble infusion rates resulted in higher mean CBRs over the 2.4-s
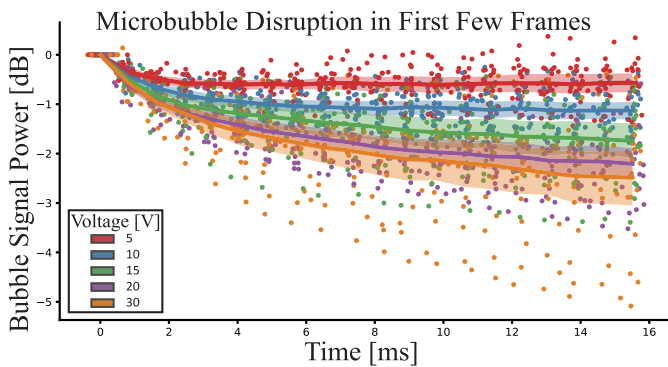
Fig. 6. Mean LV microbubble signal intensity decreased in the first 20 frames (80 acquisitions) after HFR imaging started (1.2-ml/min infusion rate). Higher transmit voltages increased the degree of signal power loss. Individual patient data are indicated with points, while the lines and shaded regions indicate the mean and 95% CI of each voltage group.

TABLE V
QUALITATIVE VECTOR FLOW SCORING [a.u.]

	0.3 ml/min	0.6 ml/min	1.2 ml/min	All
5V	2.8 [2.0, 3.7]	4.1 [3.0, 5.2]	6.1 [4.7, 7.4]	4.3 [3.6, 5.0]
10V	4.1 [2.7, 5.5]	5.1 [3.9, 6.2]	6.7 [5.6, 7.9]	5.3 [4.6, 6.0]
15V	3.6 [2.3, 4.9]	5.0 [3.8, 6.1]	6.1 [5.0, 7.2]	4.9 [4.2, 5.6]
20V	2.5 [1.3, 3.8]	4.2 [3.1, 5.3]	5.4 [4.4, 6.5]	4.1 [3.4, 4.7]
30V	1.8 [0.7, 3.0]	2.4 [1.4, 3.5]	4.7 [3.5, 5.9]	3.0 [2.3, 3.7]
All	3.0 [2.5, 6.3]	4.1 [3.6, 4.6]	5.8 [5.3, 6.3]	4.3 [4.0, 4.6]

acquisition period ($p < 0.001$). Averaging over all infusion rates, 30 V had lower CBR than 10 V ($p = 0.013$). Significance between voltage groups per infusion rate is shown by the horizontal bars in Fig. 5.

2) Microbubble Disruption: Higher transmit voltages resulted in more microbubble disruption ($p < 0.0001$), as visualized by analyzing the intracavity signal levels in the first 20 imaging frames for the 1.2-ml/min infusion rate sequences (see Fig. 6). After 20 frames (16 ms), the signal level had dropped by 0.6 dB [0.4 dB, 0.8 dB], 1.1 dB [0.9 dB, 1.3 dB], 1.7 dB [1.4 dB, 2.1 dB], 2.2 dB [1.9 dB, 2.6 dB], and 2.5 dB [1.9 dB, 3.1 dB] for 5-, 10-, 15-, 20-, and 30-V transmit voltages, respectively.

The effect of transmit voltage and UCA infusion rate on ventricular opacification and microbubble disruption is visualized in Movie 1 in the Supplementary Material.

B. Vector Flow Quality

1) Qualitative Comparison: The qualitative scores are summarized in Table V and Fig. 7. Similar to the CBR results, increasing UCA infusion rate resulted in increasing qualitative scores (p-value < 0.0001). Averaging across infusion rates, significant differences were found between: 5 and 10 V ($p = 0.008$); 5 and 30 V ($p < 0.001$); 10 and 20 V ($p = 0.001$); 10 and 30 V ($p < 0.0001$); 15 and 20 V ($p = 0.02$); 15 and

30 V ($p = 0.001$); and 20 and 30 V ($p = 0.002$). Significance between voltage groups per infusion rate is shown by the horizontal bars in Fig. 7(a).

The reliability of the qualitative scoring (Cohen's kappa statistic) was 74% and 63% for intraobserver and interobserver analyses, respectively [see Fig. 7(b)]. Examples of the echoPIV results using a subset of the CEUS settings are shown in Fig. 8 (animated version in Movie 2 in the Supplementary Material).

The mean scores for each of the criteria listed in Table III are presented as heat maps in Fig. 1 in the Supplementary Material.

2) Comparison With PW Doppler: Only the 1.2-ml/min UCA infusion rate acquisitions are shown (see Figs. 9 and 10), as lower infusion rates did not produce statistically significant regressions. Out of the 95 acquisitions using the 1.2-ml/min infusion rate, the inflow and outflow could not be seen in 13 (14%) and 29 (31%) acquisitions, respectively. The most common reasons for lack of visibility included planar misalignment, acoustic shadowing from the ribs, or poor acoustic coupling with the skin.

Linear regressions of the maximum echoPIV velocities during inflow and outflow are plotted against the peak PW Doppler velocities for the maximum (see Fig. 9) and mean (see Fig. 10) spectral tracings. Overall, the comparison with the mean velocity spectral tracing produced regression slopes that were closer to unity than the maximum velocity spectral tracing. Agreement between echoPIV and PW Doppler was also stronger for inflow than outflow, with higher r^2 values, slopes, and y-intercepts closer to zero. For inflow, the 15-V acquisitions performed best overall, with the highest r^2 values (max tracing = 0.77 and mean tracing = 0.68) and slopes (max tracing = 0.83 and mean tracing = 0.99). For outflow, the 20-V acquisitions performed best, with the highest r^2 (max tracing = 0.54 and mean tracing = 0.51) values and slopes (max tracing = 0.74 and mean tracing = 0.77).

IV. DISCUSSION

We have demonstrated that HFR echoPIV is feasible in patients with heart failure due to different aetiologies and have assessed the influence of UCA infusion rate and transmit voltage on the image and vector flow quality. We found that the highest infusion rate tested (1.2 ml/min of the 1:3 UCA dilution) was optimal for image and vector flow quality, where lower infusion rates had lower CBRs, especially in systole after a relatively long period of microbubble disruption. We also found that the lowest (5 V) and highest (30 V) transmit voltages performed the worst in terms of vector flow quality and accuracy.

A. Feasibility

Out of the 19 patients that obtained HFR CEUS recordings, 14 obtained at least one acquisition with qualitative scores higher than five out of ten (see Fig. 11). Of the five patients that did not achieve at least five out of ten scores, no particular pathology occurred more often than the others. The main reasons for the low scoring in these patients were low SNR in
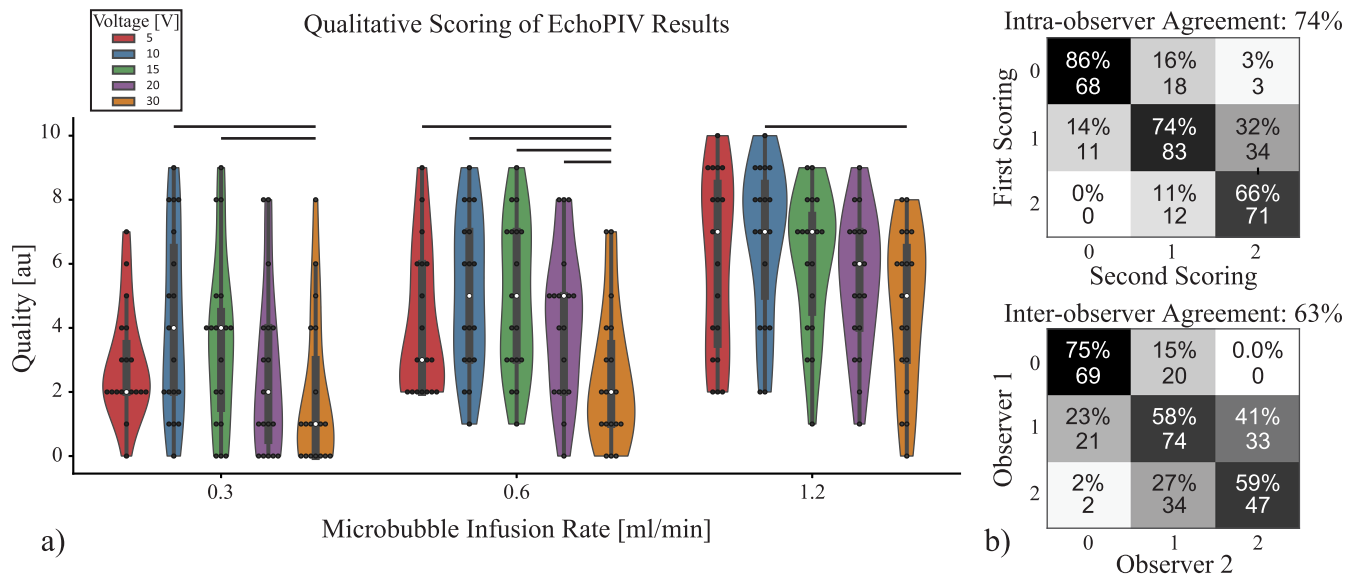
Fig. 7. Qualitative assessment of echoPIV results. (a) Scoring distribution per group, where higher concentrations scored higher on average and 30-V transmit voltage scored lowest on average. Black horizontal bars indicate statistically significant differences. Violin plots indicate kernel density estimates of the data points (black dots). White circles indicate the median of each group. (b) Confusion matrices for intraobserver and interobserver reliability (top values indicate percentage in each bin, and bottom values the count—out of 15 setting combinations × 4 patients × 5 criteria = 300).
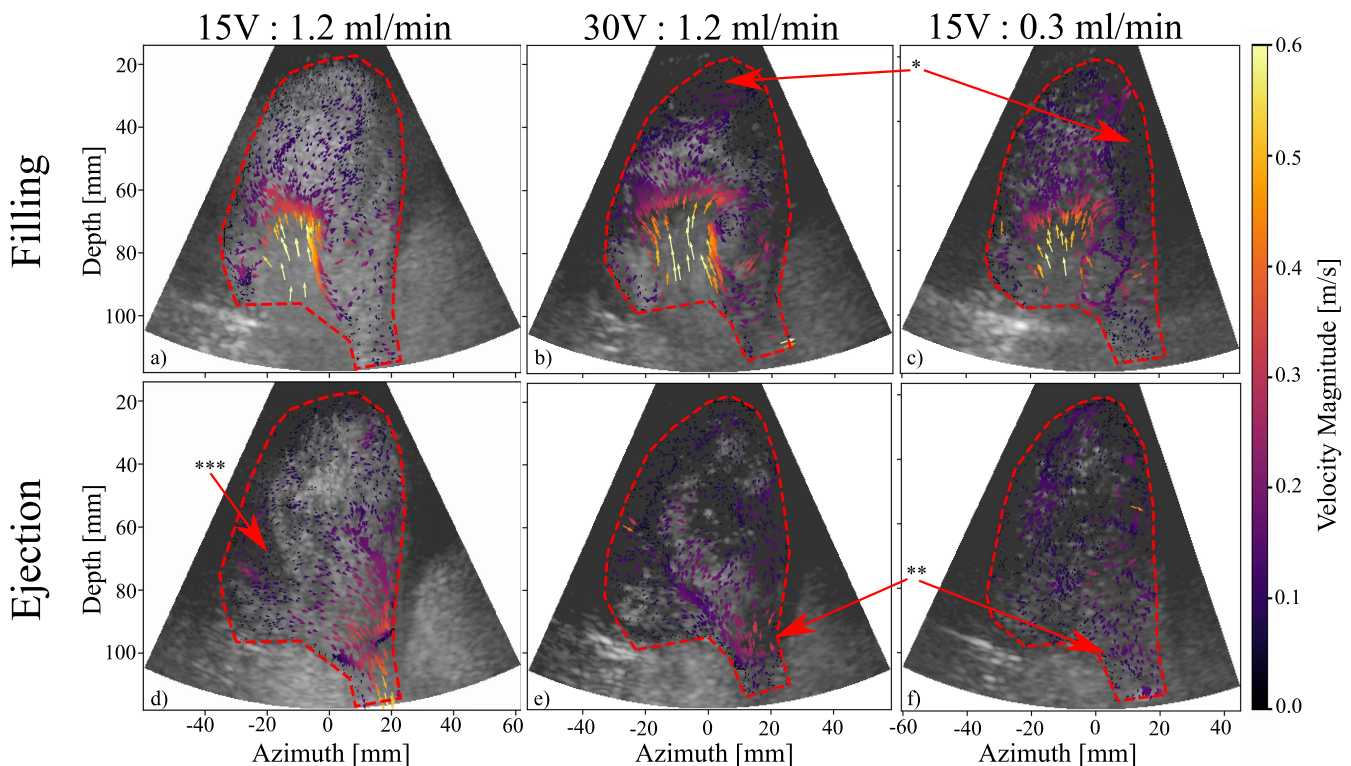
Fig. 8. Examples of echoPIV results during filling (a)–(c) and ejection (d)–(f) in a patient (with exemplary image quality) when using different CEUS parameters (columns). Tracking of the transmitral jet is similar between settings, but low signal levels are observed in the high voltage and low concentration settings (b) and (c):*. Ejection velocities are higher for the mid-range voltage and high infusion rate (d), than the high voltage or low infusion rate settings (e) and (f):** .***Papillary muscle. See Supplementary Movie 2 ▣ for animations of this figure.

the basal region (resulting in noisy inflow and outflow vectors), planar misalignment, or entire regions of the LV being hidden due to rib shadowing or clutter.

We also found that inflow was visible more often than outflow (see Figs. 9 and 10 and Fig. 1 in the Supplementary

Material). The reason for the lower visibility of outflow in this study is not certain but may be due to: 1) angle of the outflow tract when viewed in the apical three-chamber view (outflow is angled out-of-plane and, thus, underestimated or untracked); 2) the deeper placement of the LVOT

Comparison with *maximum* tracing of PW Doppler spectra

Voltage: 5V	Inflow	Outflow
r²	0.03	0.27
p-value	0.50	0.08
int. [m/s]	0.41	0.07
slope	0.15	0.45

Voltage: 10V	Inflow	Outflow
r²	0.77	0.16
p-value	<0.001	0.18
int. [m/s]	0.02	0.17
slope	0.76	0.47

Voltage: 15V	Inflow	Outflow
r²	0.77	0.41
p-value	<0.001	0.02
int. [m/s]	-0.05	0.12
slope	0.83	0.52

Voltage: 20V	Inflow	Outflow
r²	0.73	0.54
p-value	<0.001	0.003
int. [m/s]	0.17	-0.07
slope	0.55	0.74

| Voltage: 30V	Inflow	Outflow
r²	0.60	0.05
p-value	<0.001	0.45
int. [m/s]	0.01	0.32
slope	0.76	0.19

(a) (b) (c) (d) (e)

Fig. 9. (a)–(e) Regressions of maximum echoPIV and the peak *maximum* tracing of the PW Doppler spectra for inflow (orange circles) through the MV and outflow (cyan crosses) through the LVOT for increasing transmit voltage. Measured at 1.2-ml/min infusion rate, the only infusion rate with statistically significant regressions. It can be seen that echoPIV underestimates the maximum velocities compared with spectral Doppler. Observations, where inflow or outflow was not visible in the echoPIV acquisitions, were excluded. The shaded area indicates 95% CI.

Comparison with *mean* tracing of PW Doppler spectra

Voltage: 5V	Inflow	Outflow
r²	0.08	0.21
p-value	0.28	0.13
int. [m/s]	0.35	0.14
slope	0.28	0.43

Voltage: 10V	Inflow	Outflow
r²	0.71	0.19
p-value	<0.001	0.14
int. [m/s]	0.02	0.16
slope	0.92	0.55

Voltage: 15V	Inflow	Outflow
r²	0.68	0.51
p-value	<0.001	0.006
int. [m/s]	-0.04	0.10
slope	0.99	0.63

Voltage: 20V	Inflow	Outflow
r²	0.62	0.51
p-value	<0.001	0.004
int. [m/s]	0.19	-0.01
slope	0.64	0.77

Voltage: 30V	Inflow	Outflow
r²	0.60	0.04
p-value	<0.001	0.50
int. [m/s]	0.01	0.35
slope	0.90	0.18

(a) (b) (c) (d) (e)
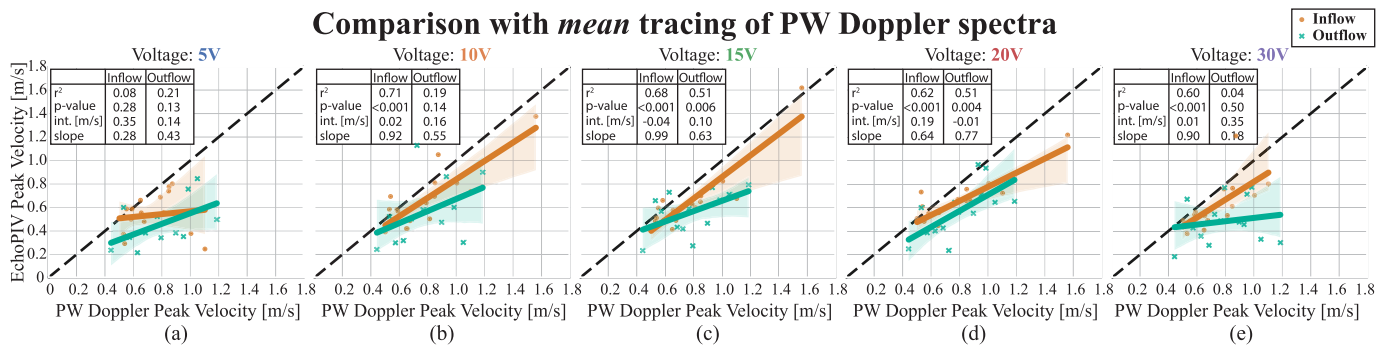
Fig. 10. (a)–(e) Regressions of maximum echoPIV and the peak *mean* tracing of the PW Doppler spectra for inflow (orange circles) through the MV and outflow (cyan crosses) through the LVOT for increasing transmit voltage. Better agreement is observed between echoPIV and the mean velocities in the sample volume of the PW spectra than with the maximum tracing (see Fig. 9). Measured at 1.2-ml/min infusion rate, the only infusion rate with statistically significant regressions. Observations, where inflow or outflow was not visible in the echoPIV acquisitions, were excluded. The shaded area indicates 95% CI.
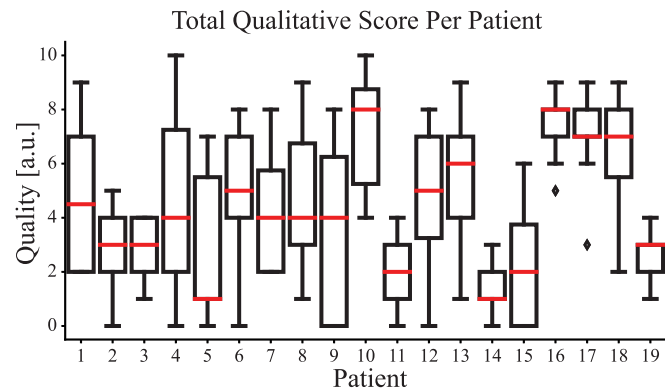
Fig. 11. Total score obtained per patient for the qualitative assessment. Note that one patient is missing due to voluntary withdrawal. Red lines indicate median, boxes extend to 25th and 75th percentiles, and whiskers indicate the range excluding samples (♦) outside of 1.5 times the interquartile range.

in the apical three-chamber view than the inflow jet, resulting in lower SNR and resolution; and 3) the small diameter of the LVOT (relative to the LV in the region of the inflow jet), which would result in higher side-lobe levels from the surrounding vessel/tissue (increased clutter) and would also complicate aligning the scan plane to the central cross section of the outflow tract–exacerbating point 1.

These view issues could likely have been avoided if real-time feedback on the HFR CEUS image quality could be obtained. In this study, the sonographer was not able to view the resulting HFR recordings after acquisition due to the excessive image reconstruction time. Beamforming on graphical processing units (GPUs) and/or data decimation may provide the image reconstruction rates required to display the captured HFR CEUS data immediately after acquisition. Expanding to 3-D VFI would also provide a potential solution to the out-of-plane flow issues [7], [32].

B. Image Quality

Higher infusion rates resulted in higher CBR, on average, over the whole acquisition period (see Fig. 5). The highest transmit voltage (30V) had the lowest CBR, which can be attributed to: 1) higher tissue intensity caused by nonlinear propagation, reducing the effectiveness of the pulse-inversion technique for selectively suppressing tissue backscatter and 2) increased microbubble disruption (see Fig. 6).

Other HFR CEUS studies have also shown similar trends between acoustic pressure (transmit voltage) and microbubble disruption when using diverging/plane wave imaging and *in vitro* [28], [29], [33] and *in vivo* in the abdominal aorta [20].

In conventional (line-scanning-based imaging) echoPIV, the reported UCA dosage varies between 0.01 and 6 ml/min for continuous infusion [34]–[36] and a consistent 0.1–0.2 ml for

bolus administration [22], [23], [37]–[39]. The reported MI values used in conventional echoPIV studies are much higher (MI = 0.1–0.7) than those used in HFR echoPIV.

In order to perform echoPIV, which involves tracking the microbubble intensities over time, it is necessary to maximize CBR while minimizing microbubble disruption. For this purpose, we found that the highest infusion rate investigated (1.2 ml/min) and a relatively low transmit voltage (10–15V) were optimal. However, the optimal transmit voltage will likely vary between patients and imaging views, so it is better to preview the beamformed HFR CEUS sequence after acquisition to visually verify that CBR is sufficient while still minimizing microbubble disruption.

C. Vector Flow Quality

Similar to image quality, higher UCA infusion rates resulted in better quality velocity estimation results both qualitatively (see Section III-B1) and quantitatively (see Section III-B2). We also see that the highest transmit voltage (30 V) performed the worst qualitatively, with high clutter levels that often interfered with the flow tracking. The optimal transmit voltages found were between 10 and 20 V, with 10 V performing best in the qualitative scoring overall.

In the echoPIV and PW Doppler-derived maximum velocity comparison (during inflow and outflow), we found that the 0.3- and 0.6-ml/min concentrations produced no significant linear relationships, indicating inconsistent echoPIV accuracy using these infusion rates. For the 1.2-ml/min infusion rate, we found that the 5-V acquisitions resulted in poor accuracy, despite very low clutter levels, indicating that CBR was an issue. For the 30-V transmit, although clutter levels were high, we found good agreement with the PW Doppler traces for inflow but not for outflow. This discrepancy is likely due to microbubble disruption, as, during filling, the microbubbles are replenished and tracking is improved by high CBR, whereas, during outflow, significant microbubble disruption has already occurred, and poor CBR is available for tracking. Another factor worth considering is the higher clutter levels observed in the 30-V acquisitions, where high sidelobe levels from surrounding tissue interfere with the flow signal in the outflow tract.

Overall, the 15- and 20-V acquisitions performed best in the PW Doppler comparison, where the 10 V resulted in a nonsignificant regression for outflow. We found echoPIV underestimated peak velocities increasingly with velocity magnitude (regression slopes <1.0; see Fig. 9), similar to the findings of Nyrnes *et al.* [5] when using blood speckle tracking. Underestimation is expected as echoPIV is a block-matching technique (similar to blood speckle tracking) that estimates the bulk displacement present in the interrogation kernel, which, for nonuniform flow, will always be lower in magnitude than the peak displacement present in the kernel. If we instead compare the peak echoPIV velocities to the peak PW Doppler velocities obtained from the mean velocity tracing of the Doppler spectrum (see Fig. 10), then the agreement is much stronger, as expected.

In our previous work [16], where we compared HFR echoPIV with optical PIV in a dynamic LV *in vitro* model,

we found that echoPIV achieved normalized root-mean-squared errors (NRMSEs) of 16% for the high velocities (>30 cm/s) present in the transmitral filling jet. In that study, we were also able to assess the similarity in flow patterns, which was good for the high energy flow patterns. In addition, we have compared HFR echoPIV with 4-D flow MRI in abdominal aortic flow quantification in healthy volunteers [18], also finding good agreement between the two modalities with peak velocity differences ranging between 8.5% and 17%. In that previous study, we found that the lowest UCA bolus concentration was optimal; however, this conclusion was based on optimization of systolic VFI only, whereas further investigation [20] found that higher bolus concentrations were favorable during cardiac phases with less UCA replenishment, where microbubble disruption was more prevalent—similar to the findings of this study.

D. Limitations

While great care was taken to ensure that the same view was preserved between acquisitions, perfect alignment was impossible. Thus, it should be kept in mind that some of the measurement variations can be attributed to variation in the imaging plane (caused by probe placement, probe motion, and breathing motion). This especially applies to the comparison with PW Doppler, which was obtained with the clinical scanner before contrast infusion. In an effort to minimize view changes, we structured the acquisition protocol such that the probe only had to be removed and replaced between infusion rate changes (to check that the new UCA concentration had been reached with the clinical ultrasound system).

It is still unclear if infusion rates higher than 1.2 ml/min would have provided better image and vector flow quality, as they were not tested. However, too high concentrations are known from clinical CEUS measurements to cause acoustic shadowing and nonlinear propagation artifacts [25], [26], which are expected to degrade tracking quality.

This study had a depth limit of 12 cm; however, this was only due to our fixed PRF implementation, which was used to keep the frame rate the same for all acquisitions. In the future, the PRF can be linked to the maximum depth of interest (based on the two-way transit time).

E. Future Improvements

While the feasibility was high in this study, it could have been further improved if immediate feedback on HFR CEUS image quality was provided to the sonographer. This would allow for bad image views to be discarded and recaptured. Increasing the beamforming speed using GPUs and/or data decimation could solve this issue in the future.

The validation of flow features was not possible in this study as the PW Doppler was obtained in only two points in the LV. Comparison with 4-D flow MRI would be a possible next step, allowing for flow comparison over the whole image slice.

Acquiring a full-field Eulerian velocity field allows for the calculation of many relevant parameters, such as vorticity [22], [34], [39], [40], kinetic energy (dissipation) [7], and relative pressure gradients [41]. It is also possible to perform

particle displacement analyses using these flow fields to simulate parameters, such as particle residence time and washout period [42], [43]. The potential of using echoPIV for the assessment of these parameters should be studied and validated in future work.

In this study, we used only two angles for coherent compounding, in an effort to reduce the amount of scatterer motion present between angles. However, the tilt and number of angles used were not systematically optimized and may offer future improvements.

V. Conclusion

We have shown that HFR echoPIV is feasible, and it can provide estimates of the high filling and ejection velocities in the LV that is consistent with PW Doppler. High UCA infusion rates provided better image quality (higher CBR) and flow tracking, with the highest infusion rate of 1.2 ml/min (of a 1:3 UCA dilution) performing best overall. Low-to-medium (10–20 V) transmit voltages performed best overall, where the lowest (5 V) and highest (30 V) had issues with SNR and clutter/microbubble disruption, respectively. However, these settings only provide a good starting point for optimization, where real-time feedback on the acquisition image quality should be used for further fine-tuning per patient and/or imaging view.

Acknowledgment

References

[1] P. Tortoli, M. Lenge, D. Righi, G. Ciuti, H. Liebgott, and S. Ricci, "Comparison of carotid artery blood velocity measurements by vector and standard Doppler approaches," *Ultrasound Med. Biol.*, vol. 41, no. 5, pp. 1354–1362, May 2015, doi: 10.1016/j.ultrasmedbio.2015.01.008.

[2] S. Holbek et al., "Real-time 2-D phased array vector flow imaging," *IEEE Trans. Ultrason., Ferroelectr., Freq. Control*, vol. 65, no. 7, pp. 1205–1213, Jul. 2018, doi: 10.1109/TUFFC.2018.2838518.

[3] K. Hansen, K. Juul, H. Møller-Sørensen, J. Nilsson, J. Jensen, and M. Nielsen, "Pediatric transthoracic cardiac vector flow imaging a preliminary pictorial study," *Ultrasound Int. Open*, vol. 5, no. 1, pp. E20–E26, Jan. 2019, doi: 10.1055/a-0656-5430.

[4] K. C. Assi et al., "Intraventricular vector flow mapping—A Doppler-based regularized problem with automatic model selection," *Phys. Med. Biol.*, vol. 62, no. 17, pp. 7131–7147, Aug. 2017, doi: 10.1088/1361-6560/aa7fe7.

[5] S. A. Nyrnes, S. Fadnes, M. S. Wigen, L. Mertens, and L. Lovstakken, "Blood speckle-tracking based on high-frame rate ultrasound imaging in pediatric cardiology," *J. Amer. Soc. Echocardiogr.*, vol. 33, no. 4, pp. 493–503, Apr. 2020, doi: 10.1016/j.echo.2019.11.003.

[6] S. Fadnes, M. S. Wigen, S. A. Nyrnes, and L. Lovstakken, "in vivo intracardiac vector flow imaging using phased array transducers for pediatric cardiology," *IEEE Trans. Ultrason., Ferroelectr., Freq. Control*, vol. 64, no. 9, pp. 1318–1326, Sep. 2017, doi: 10.1109/TUFFC.2017.2689799.

[7] M. S. Wigen et al., "4-D intracardiac ultrasound vector flow imaging–feasibility and comparison to phase-contrast MRI," *IEEE Trans. Med. Imag.*, vol. 37, no. 12, pp. 2619–2629, Dec. 2018, doi: 10.1109/TMI.2018.2844552.

[8] H. J. Vos et al., "Contrast-enhanced high-frame-rate ultrasound imaging of flow patterns in cardiac chambers and deep vessels," *Ultrasound Med. Biol.*, vol. 46, no. 11, pp. 2875–2890, Nov. 2020, doi: 10.1016/j.ultrasmedbio.2020.07.022.

[9] C. Poelma, "Ultrasound imaging velocimetry: A review," *Experim. Fluids*, vol. 58, no. 1, Jan. 2017, doi: 10.1007/s00348-016-2283-9.

[10] D. Garcia, "Introduction to speckle tracking in cardiac ultrasound imaging," in *Handbook of Speckle Filtering and Tracking in Cardiovascular Ultrasound Imaging and Video*. 2018, pp. 571–598, doi: 10.1049/pbhe013e_ch26.

[11] D. Mele et al., "Intracardiac flow analysis: Techniques and potential clinical applications," *J. Amer. Soc. Echocardiogr.*, vol. 32, no. 3, pp. 319–332, Mar. 2019, doi: 10.1016/j.echo.2018.10.018.

[12] J. Hwang and D. Simpson, "Two pulse technique for ultrasonic harmonic imaging," U.S. Patent 5 951 478 A, Sep. 14, 1999.

[13] C. S. Chapman and J. C. Lazenby, "Ultrasound imaging system employing phase inversion subtraction to enhance the image," U.S. Patent 5 632 277 A, May 27, 1997.

[14] C. H. Leow, E. Bazigou, R. J. Eckersley, A. C. H. Yu, P. D. Weinberg, and M.-X. Tang, "Flow velocity mapping using contrast enhanced high-frame-rate plane wave ultrasound and image tracking: Methods and initial *in vitro* and *in vivo* evaluation," *Ultrasound Med. Biol.*, vol. 41, no. 11, pp. 2913–2925, Nov. 2015, doi: 10.1016/j.ultrasmedbio.2015.06.012.

[15] C. H. Leow and M.-X. Tang, "Spatio-temporal flow and wall shear stress mapping based on incoherent ensemble-correlation of ultrafast contrast enhanced ultrasound images," *Ultrasound Med. Biol.*, vol. 44, no. 1, pp. 134–152, Jan. 2018, doi: 10.1016/j.ultrasmedbio.2017.08.930.

[16] J. Voorneveld et al., "High frame rate ultrasound particle image velocimetry for estimating high velocity flow patterns in the left ventricle," *IEEE Trans. Ultrason., Ferroelectr., Freq. Control*, vol. 65, no. 12, pp. 2222–2232, Dec. 2018, doi: 10.1109/TUFFC.2017.2786340.

[17] M. E. G. Toulemonde et al., "High frame-rate contrast echocardiography: In-human demonstration," *JACC, Cardiovascular Imag.*, vol. 11, no. 6, pp. 923–924, Jun. 2018, doi: 10.1016/j.jcmg.2017.09.011.

[18] S. Engelhard et al., "High-frame-rate contrast-enhanced US particle image velocimetry in the abdominal aorta: First human results," *Radiology*, vol. 289, no. 1, pp. 119–125, Oct. 2018, doi: 10.1148/radiol.2018172979.

[19] L. Nie, D. M. J. Cowell, T. M. Carpenter, J. R. Mclaughlan, A. A. Cubukcu, and S. Freear, "High-frame-rate contrast-enhanced echocardiography using diverging waves: 2-D motion estimation and compensation," *IEEE Trans. Ultrason., Ferroelectr., Freq. Control*, vol. 66, no. 2, pp. 359–371, Feb. 2019, doi: 10.1109/TUFFC.2018.2887224.

[20] J. Voorneveld et al., "High-frame-rate contrast-enhanced ultrasound for velocimetry in the human abdominal aorta," *IEEE Trans. Ultrason., Ferroelectr., Freq. Control*, vol. 65, no. 12, pp. 2245–2254, Dec. 2018, doi: 10.1109/TUFFC.2018.2846416.

[21] J. Voorneveld et al., "High-frame-rate echo-particle image velocimetry can measure the high-velocity diastolic flow patterns," *Circulat., Cardiovascular Imag.*, vol. 12, no. 4, Apr. 2019, doi: 10.1161/CIRCIMAGING.119.008856.

[22] A. Kheradvar et al., "Echocardiographic particle image velocimetry: A novel technique for quantification of left ventricular blood vorticity pattern," *J. Amer. Soc. Echocardiogr.*, vol. 23, no. 1, pp. 86–94, Jan. 2010, doi: 10.1016/j.echo.2009.09.007.

[23] C. Prinz et al., "Can echocardiographic particle image velocimetry correctly detect motion patterns as they occur in blood inside heart chambers? A validation study using moving phantoms," *Cardiovascular Ultrasound*, vol. 10, no. 1, p. 24, Dec. 2012, doi: 10.1186/1476-7120-10-24.

[24] H. Gao, P. Claus, M.-S. Amzulescu, I. Stankovic, J. D'hooge, and J.-U. Voigt, "How to optimize intracardiac blood flow tracking by echocardiographic particle image velocimetry? Exploring the influence of data acquisition using computer-generated data sets," *Eur. Heart J.-Cardiovascular Imag.*, vol. 13, no. 6, pp. 490–499, Jun. 2012, doi: 10.1093/ejechocard/jer285.

[25] C. Dietrich et al., "How to perform contrast-enhanced ultrasound (CEUS)," *Ultrasound Int. Open*, vol. 4, no. 1, pp. E2–E15, Jan. 2018, doi: 10.1055/s-0043-123931.

[26] M.-X. Tang et al., "Quantitative contrast-enhanced ultrasound imaging: A review of sources of variability," *Interface Focus*, vol. 1, no. 4, pp. 520–539, Aug. 2011, doi: 10.1098/rsfs.2011.0026.

[27] C. Tremblay-Darveau, R. Williams, P. S. Sheeran, L. Milot, M. Bruce, and P. N. Burns, "Concepts and tradeoffs in velocity estimation with plane-wave contrast-enhanced Doppler," *IEEE Trans. Ultrason., Ferroelectr., Freq. Control*, vol. 63, no. 11, pp. 1890–1905, Nov. 2016, doi: 10.1109/TUFFC.2016.2596581.

[28] M. Toulemonde, R. J. Eckersley, and M.-X. Tang, "High frame rate contrast enhanced echocardiography: Microbubbles stability and contrast evaluation," in *Proc. IEEE Int. Ultrason. Symp. (IUS)*, Sep. 2017, pp. 1–4.

[29] O. Couture, M. Fink, and M. Tanter, "Ultrasound contrast plane wave imaging," *IEEE Trans. Ultrason., Ferroelectr., Freq. Control*, vol. 59, no. 12, pp. 2676–2683, Dec. 2012, doi: 10.1109/TUFFC.2012.2508.

[30] F. Scarano and M. L. Riethmuller, "Advances in iterative multigrid PIV image processing," *Experim. Fluids*, vol. 29, no. 7, pp. S051–S060, Dec. 2000, doi: 10.1007/s003480070007.

[31] B. Y. S. Yiu, S. S. M. Lai, and A. C. H. Yu, "Vector projectile imaging: Time-resolved dynamic visualization of complex flow patterns," *Ultrasound Med. Biol.*, vol. 40, no. 9, pp. 2295–2309, Sep. 2014, doi: 10.1016/j.ultrasmedbio.2014.03.014.

[32] J. Voorneveld *et al.*, "4-D echo-particle image velocimetry in a left ventricular phantom," *Ultrasound Med. Biol.*, vol. 46, no. 3, pp. 805–817, Mar. 2020, doi: 10.1016/j.ultrasmedbio.2019.11.020.

[33] C. Tremblay-Darveau, R. Williams, L. Milot, M. Bruce, and P. N. Burns, "Combined perfusion and Doppler imaging using plane-wave nonlinear detection and microbubble contrast agents," *IEEE Trans. Ultrason., Ferroelectr., Freq. Control*, vol. 61, no. 12, pp. 1988–2000, Dec. 2014, doi: 10.1109/TUFFC.2014.006573.

[34] L. Agati *et al.*, "Quantitative analysis of intraventricular blood flow dynamics by echocardiographic particle image velocimetry in patients with acute myocardial infarction at different stages of left ventricular dysfunction," *Eur. Heart J. Cardiovascular Imag.*, vol. 2, pp. 1203–1212, Jun. 2014, doi: 10.1093/ehjci/jeu106.

[35] S. Kutty *et al.*, "Effects of right ventricular hemodynamic burden on intraventricular flow in tetralogy of fallot: An echocardiographic contrast particle imaging velocimetry study," *J. Amer. Soc. Echocardiogr.*, vol. 27, no. 12, pp. 1311–1318, Dec. 2014, doi: 10.1016/j.echo.2014.09.016.

[36] P. P. Sengupta *et al.*, "Left ventricular isovolumic flow sequence during sinus and paced rhythms," *J. Amer. College Cardiol.*, vol. 49, no. 8, pp. 899–908, Feb. 2007, doi: 10.1016/j.jacc.2006.07.075.

[37] H. Abe *et al.*, "Contrast echocardiography for assessing left ventricular vortex strength in heart failure: A prospective cohort study," *Eur. Heart J.-Cardiovascular Imag.*, vol. 14, no. 11, pp. 1049–1060, Nov. 2013, doi: 10.1093/ehjci/jet049.

[38] G. Goliasch *et al.*, "CRT improves LV filling dynamics," *JACC, Cardiovascular Imag.*, vol. 6, no. 6, pp. 704–713, Jun. 2013, doi: 10.1016/j.jcmg.2013.04.004.

[39] G.-R. Hong *et al.*, "Characterization and quantification of vortex flow in the human left ventricle by contrast echocardiography using vector particle image velocimetry," *JACC, Cardiovascular Imag.*, vol. 1, no. 6, pp. 705–717, Nov. 2008, doi: 10.1016/j.jcmg.2008.06.008.

[40] R. Faludi *et al.*, "Left ventricular flow patterns in healthy subjects and patients with prosthetic mitral valves: An *in vivo* study using echocardiographic particle image velocimetry," *J. Thoracic Cardiovascular Surg.*, vol. 139, no. 6, pp. 1501–1510, Jun. 2010, doi: 10.1016/j.jtcvs.2009.07.060.

[41] S. Fadnes, K. Sørensen, S. A. Nyrnes, M. S. Wigen, and L. Lovstakken, "Intraventricular pressure gradients-vector flow imaging versus color M-mode," in *Proc. IEEE Int. Ultrason. Symp. (IUS)*, Sep. 2020, pp. 1–4.

[42] Y. Benito *et al.*, "Age-dependence of flow homeostasis in the left ventricle," *Frontiers Physiol.*, vol. 10, p. 485, Apr. 2019, doi: 10.3389/fphys.2019.00485.

[43] L. Rossini *et al.*, "A clinical method for mapping and quantifying blood stasis in the left ventricle," *J. Biomech.*, vol. 49, no. 11, pp. 2152–2161, Jul. 2016, doi: 10.1016/j.jbiomech.2015.11.049.

Lana B. H. Keijzer was born in Leiderdorp, The Netherlands, in 1992. She received the B.Sc. and M.Sc. degrees in applied physics with a specialization in medical and acoustical waveform imaging and the M.Sc. degree in management of technology from the Delft University of Technology, Delft, The Netherlands, in 2013, 2015, and 2016, respectively, and the Ph.D. degree from the Department of Biomedical Engineering, Thorax Center, Erasmus University Medical Center, Rotterdam, The Netherlands, in 2020. Her thesis focuses on cardiac shear wave elastography measurements.

She is currently working as a clinical physicist in training.
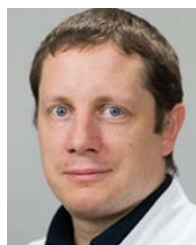
Mihai Strachinaru received the M.D. degree and his cardiology specialization from the "Carol Davila" University of Medicine and Pharmacy, Bucharest, Romania, in 2001 and 2008, respectively, and the Ph.D. degree in shear wave echocardiography from the Department of Biomedical Engineering, Erasmus University Medical Center (Erasmus MC), Rotterdam, The Netherlands, in 2020.

He then moved on to work as a cardiologist in France from 2008 to 2009, Belgium from 2009 to 2016, and The Netherlands from 2016 to 2019. During this period, he developed a keen interest in cardiac noninvasive imaging, especially echocardiography. He currently holds Romanian, French, and European certifications in transthoracic and transesophageal echocardiography. He is currently a Postdoctoral Researcher with the Erasmus MC and an Intensive Care Cardiologist with the CHIREC Hospital, Brussels, Belgium. His research interests include high-frame-rate ultrasound imaging in all its aspects: 2-D and 3-D, cardiac shear waves, ultrafast Doppler, contrast imaging, and related preclinical and clinical applications.

Daniel J. Bowen was born in 1986. He received the B.Sc. degree in clinical physiology from Middlesex University, London, U.K., in 2013.

He trained in echocardiography at the Papworth Hospital, Cambridge, U.K., from 2014 to 2017, and the Colchester General Hospital, Colchester, U.K., from 2010 to 2014. Since 2018, he has been a Research Echocardiographer with the Department of Cardiology, Erasmus University Medical Center (Erasmus MC), Rotterdam, The Netherlands. He collaborates with the Department of Biomedical Engineering, Erasmus MC, to aid the research and development of novel ultrasound modalities.

Jason Voorneveld was born in Johannesburg, South Africa, in 1987. He received the B.Sc. degree in electromechanical engineering and the M.Sc. degree in biomedical engineering from the University of Cape Town, Cape Town, South Africa, in 2009 and 2014, respectively, and the Ph.D. degree in biomedical engineering from the Erasmus University Medical Center (Erasmus MC), Rotterdam, The Netherlands, in 2019.

He currently holds a postdoctoral position at Erasmus MC. His research interests include high-frame-rate ultrasound imaging, blood-flow imaging, and contrast-enhanced ultrasound imaging.

Ferit Onur Mutluer was born in Istanbul, Turkey, in 1983. He received the M.D. degree from Hacettepe University Faculty of Medicine, Ankara, Turkey, in 2007. He is currently pursuing the Ph.D. degree with the Erasmus University Medical Center (Erasmus MC), Rotterdam, The Netherlands.

He received his interventional cardiology training from Siyami Ersek Hospital, Istanbul. He is currently an Associate Professor with Istinye University, Istanbul. His current research focuses on speckle tracking echocardiography, adult congenital heart disease, and noninvasive flow visualization.

Antonius F. W. van der Steen (Fellow, IEEE) received the M.Sc. degree in applied physics from the Delft University of Technology (TU Delft), Delft, The Netherlands, in 1989, and the Ph.D. degree in medical sciences from the University of Nijmegen, Nijmegen, The Netherlands, in 1994.

Since 1994, he has been with the Thorax Centre, Erasmus University Medical Center (Erasmus MC), Rotterdam, The Netherlands, where he is currently a Full Professor and the Head of Biomedical Engineering since 2002. Since 2013, he has been a Full Professor of applied physics with TU Delft. Since 2013, he is also an Honorary Visiting Professor with the Chinese Academy of Sciences, Shenzhen Institute of Advanced Technology, Shenzhen, China. He is a Cofounder and the Past Chairman of the Medical Delta: a collaboration between Erasmus MC, TU Delft, and the Leiden University Medical Centre, Leiden, The Netherlands, working on technical solutions for sustainable health. His expertise is mainly in diagnostic cardiologic imaging devices with an emphasis on echography. His current research interests are focused on image-guided catheter-based treatment of atherosclerosis, ultrasound contrast agents, ultrasound transducers, and vascular biomechanics.

Dr. van der Steen is also a member of the Netherlands Academy of Engineering (AcTI) and a Board Member of the Netherlands Academy of Sciences (KNAW). He is also a fellow of the European Society of Cardiology. He was a recipient of the 2000 NWO PIONIER Technical Sciences and the 2007 Simon Stevin Master. He was the IEEE UFFC Distinguished Lecturer from 2011 to 2012. From 2014 to 2017, he was the Chairman of the Board of the Dutch Technology foundation and the NWO Technical Sciences.

Folkert J. Ten Cate was born in 1948. He received the M.D. degree from the Erasmus University Medical Center, Rotterdam, The Netherlands, in 1972.

He defended his Ph.D. dissertation and became a Board-certified cardiologist in 1978. Since 1978, he has been a Staff Member of the Thoraxcenter, Erasmus University Medical Center, where his research is focused on the clinical applications of novel 2-D and 3-D ultrasound transducers. He was one of the first investigators worldwide, who took an interest in microbubbles for contrast echocardiography. He has been a Co-Organizer for the European Symposium of Ultrasound Contrast Imaging, Rotterdam, since 1996. In the last years, his main interest has been in the research of microbubbles for gene and drug delivery.

Nico de Jong (Member, IEEE) received the M.Sc. degree in physics specialized in the field of pattern recognition from the Delft University of Technology, Delft, The Netherlands, in 1978, and the Ph.D. in acoustic properties of ultrasound contrast agents from the Department of Biomedical Engineering, Thorax Center, Erasmus University Medical Center (Erasmus MC), Rotterdam, The Netherlands, in 1993.

In 2003, he joined the University of Twente, Enschede, The Netherlands, as a part-time Professor. He currently teaches at Technical Universities and Erasmus MC. Since 1980, he has been a Staff Member with the Thorax Center, Erasmus MC. Since 2011, he has been a Professor of molecular ultrasonic imaging and therapy with Erasmus MC and the Delft University of Technology. Since 2015, he has been the part-time Head of the Department of Acoustical Waveform Imaging, Delft University of Technology. He has been a Promotor of 21 Ph.D. students and is currently co-supervising 11 Ph.D. students.

Dr. de Jong is also the Organizer of the Annual European Symposium on Ultrasound Contrast Imaging, Rotterdam. He is on the Safety Committee of the World Federation of *Ultrasound in Medicine and Biology* and is an Associate Editor of *Ultrasound in Medicine and Biology* and a Guest Editor of the special issues of different journals.

Hendrik J. Vos (Member, IEEE) received the M.Sc. degree in applied physics from the Delft University of Technology, Delft, The Netherlands, in 2004, and the Ph.D. degree from the Department of Biomedical Engineering, Erasmus MC, Rotterdam, The Netherlands, in 2010.

He worked as a Postmaster Researcher with the University of Florence, Florence, Italy, and as a Contract Researcher for the petrochemical industry on cutting-edge ultrasonic solutions. He is currently an Associate Professor with Erasmus MC and the Delft University of Technology. He received a Dutch NWO-TTW-VIDI Personal Grant in 2018. His research interests include acoustical array technology for biomedical imaging in all its aspects: transducers, 2-D and 3-D beamforming, cardiac shear waves, ultrafast Doppler, contrast imaging, and related subclinical and clinical studies.

Annemien E. van den Bosch is currently a Cardiologist with the Erasmus University Medical Center, Rotterdam, The Netherlands. Her clinical work and research involve adult congenital heart disease, echocardiography, and pulmonary hypertension. She is also involved in basic and translational research on new echocardiographic techniques as high-frame-rate echocardiography, the development of multiplane echocardiography, and the value of imaging biomarkers in the follow-up of patients with congenital heart disease.

Johan G. Bosch (Member, IEEE) received the M.Sc. degree in electrical engineering from the Eindhoven University of Technology, Eindhoven, The Netherlands, in 1985, and the Ph.D. degree from the Leiden University Medical Center, Leiden, The Netherlands, in 2006.

He is currently an Associate Professor and a Staff Member with Thoraxcenter Biomedical Engineering, Department of Cardiology, Erasmus University Medical Center, Rotterdam, The Netherlands. He is a (Co)PI of projects on 3-D ultrasound image formation, transducer development, 2-D and 3-D cardiovascular imaging, and flow and tissue stiffness assessment using novel ultrasound approaches. His research interests include echocardiographic image processing, transducer development, and novel ultrasound techniques for image formation and functional imaging.